POLITECNICO DI TORINO
Repository ISTITUZIONALE

Accurate Simulation Model of Variable Flux Machines under Asymmetrical Demagnetization without FEA Co-simulation

Original
Accurate Simulation Model of Variable Flux Machines under Asymmetrical Demagnetization without FEA Co-simulation / Garino, R., Pescetto, P., Chen, C., Ferrari, S., Diana, M., Pellegrino, G.. - ELETTRONICO. - (2025), pp. 1-8. (2025 IEEE Energy Conversion Conference Congress and Exposition (ECCE) Philadelphia (USA) 19-23 October 2025) [10.1109/ecce58356.2025.11260258].

Availability:
This version is available at: 11583/3007094 since: 2026-01-29T15:59:50Z

Publisher:
IEEE

Published
DOI:10.1109/ecce58356.2025.11260258

Terms of use:

This article is made available under terms and conditions as specified in the corresponding bibliographic description in the repository

Publisher copyright
IEEE postprint/Author's Accepted Manuscript

©2025 IEEE. Personal use of this material is permitted. Permission from IEEE must be obtained for all other uses, in any current or future media, including reprinting/republishing this material for advertising or promotional purposes, creating new collecting works, for resale or lists, or reuse of any copyrighted component of this work in other works.

(Article begins on next page)

26 November 2026

Accurate Simulation Model of Variable Flux Machines under Asymmetrical Demagnetization without FEA Co-simulation

Raffaele Garino
Energy Department Galileo Ferraris
Politecnico di Torino
Torino, Italy
raffaele.garino@polito.it

Paolo Pescetto
Energy Department Galileo Ferraris
Politecnico di Torino
Torino, Italy
paolo.pescetto@polito.it

Chen Chen
Energy Department Galileo Ferraris
Politecnico di Torino
Torino, Italy
chen_chen@polito.it

Simone Ferrari
Energy Department Galileo Ferraris
Politecnico di Torino
Torino, Italy
simone.ferrari@polito.it

Michela Diana
Electric Driveline Department
Volvo Cars
Göteborg, Sweden
michela.diana@volvocars.com

Gianmario Pellegrino
Energy Department Galileo Ferraris
Politecnico di Torino
Torino, Italy
gianmario.pellegrino@polito.it

***Abstract*—Variable-Flux Permanent Magnet Synchronous Machines (VFMs) employ low-coercivity permanent magnets whose Magnetization State (MS) can be dynamically adjusted through controlled current pulses. Achieving accurate MS regulation under load, while avoiding torque discontinuities, requires injecting current pulses that are not aligned with the magnets, resulting in asymmetric demagnetization. These nonlinear magnetization and demagnetization dynamics are not captured by conventional control-oriented models, and are typically analyzed using computationally expensive finite element analysis (FEA) co-simulations, which are impractical for control development and calibration.**

This paper presents an enhanced, high-fidelity dynamic model of VFMs, optimized for efficient simulation in Matlab-Simulink. The model leverages precomputed lookup tables, obtained from FEA or experimental data, including inverse flux linkage characteristics and novel remagnetization and demagnetization maps along orthogonal (x–y) magnet axes, enabling accurate representation of asymmetric PM behavior. Validation against transient FEA simulations demonstrates that the proposed model achieves comparable accuracy while reducing simulation time from 124 minutes to just 14 seconds, making it well suited for real-time-oriented applications such as controller design and system calibration.

***Index Terms*—Variable Flux Machines, Memory Motors, Motor Modeling, Flux Maps, Irreversible Demagnetization, Computational Efficiency.**

I. Introduction

The growing demand for electric vehicles (EVs) has intensified the need for high-performance, energy-efficient electric machines. Currently, large part of the EV traction motors rely on Permanent Magnet (PM) Synchronous Motors (PMSMs) embedding rare-earth based magnets, normally NdFeB, to achieve high power density and efficiency [1]–[4]. However, the extraction and processing of rare earth elements pose significant environmental and geopolitical concerns. Furthermore, the global supply chain for rare earth materials is heavily concentrated, raising concerns about long-term sustainability, price volatility, and resource security [5]. These challenges have prompted researchers and industry to explore alternative machine topologies that reduce or eliminate reliance on rare earth magnets without compromising the machine performance [6]–[9]. Among the feasible alternatives, Variable Flux Machines (VFMs) have emerged as a promising rare-earth-free solution [10], enabling extended speed range and mission profile optimized efficiency by dynamically adjusting their PM flux. This is attractive for EV traction motor-drives [11]–[16], as well as for duty-cycle based applications such as washing machines [17]–[19].

In a VFM, the PM flux is regulated through magnetization and demagnetization current pulses compatible with inverter ratings. A high PM magnetization is imposed in the low speed range, thus maximizing the torque capability. At higher speeds, when voltage limitation occurs, field weakening operation is conveniently achieved by partially demagnetizing the PM. The

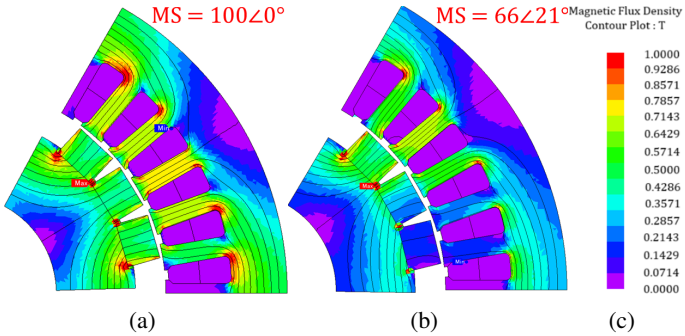

Fig. 1: Open circuit FEA results. (a) symmetric magnetization state. (b) deviated **MS** after asymmetric demagnetization.

Magnetization State (MS) manipulation can be achieved by using d-axis current pulses, i.e. parallel to the PM direction, to maintain a uniform PM magnetization, but this requires interrupting the torque during the MS transient. Conversely, using a dedicated mix of d- and q-axis currents for the de- or re-magnetization pulse permits to maintain torque continuity, but it may alter the PM flux direction, thus compromising control accuracy and stability. An example of asymmetrical demagnetization is given in Fig. 1.

In recent years, several studies have investigated VFMs, proposing advances in machine design, modeling, and control strategies. Finite Element Analysis (FEA) is a standard practice in the motor design stage, including machine topology selection and electromagnetic design optimization. FEA simulations can accurately represent the nonlinear magnetic behavior of the machine, including saturation phenomena and PM demagnetization and remagnetization [20], at the cost of high computational burden and simulation time. This is generally accepted at the motor design stage, when extensive FEA simulations can be run overnight. Conversely, when dealing with motor control development and calibration of standard PMSMs, fast simulation models are necessary, as a high number of simulations need to be executed in a reasonable time. Fast simulation models for control development, e.g. implemented in Matlab-Simulink, normally capture the magnetic saturation phenomena by means of embedded Look-Up-Tables (LUTs), but the PM demagnetization, inherently present in VFMs, is hardly represented. For this reason, VFM models for control development often exploit FEA-based simulations or FEA-Simulink co-simulations [21]–[23], accepting the associated high computational burden and execution time. This is a significant bottleneck for the VFM control development.

Recent works have proposed simplified and time-efficient dynamic models of VFMs aimed at enabling fast simulations without compromising the accuracy needed to capture the machine's magnetic behavior. In [24], the VFM is modeled using FEA pre-calculated LUTs of flux, inductance and torque, computed as a function of current amplitude and rotor position. The model is implemented on an FPGA-based P-HIL platform. Instead in [25] the VFM is modeled based on experimental measurements of inductance, mutual inductances and magnetization and demagnetization characteristics using current pulses on the d-axis at locked rotor. The magnet flux is then computed through spline-interpolated LUTs derived from these measurements. A dynamic VFM model fully based on Matlab/Simulink was proposed in [26], which uses magnetization and remagnetization maps to track the magnetization state of the PMs. Based on this state, the model employs inverse flux LUTs computed for different values of MS. However, all these models have so far exclusively assumed symmetric magnetization of the PMs.

To overcome these limitations, this paper introduces an improved VFM analytical model and its implementation in fast simulation environment, able to capture symmetric and asymmetric PM demagnetization. The model is based on pre-calculated saturation and magnetization LUTs, either obtained via FEA or by experiments, and it is directly executable in Simulink or in equivalent simulation environments. The developed model is compared against conventional FEA-based co-simulation approach, demonstrating a reduction of the simulation time by two orders of magnitude while maintaining high fidelity in steady state and minor discrepancy during sharp transients.

II. Motor Under Test and New VFM Model

The Motor Under Test (MUT) is a Surface-mounted PM (SPM) synchronous machine embedding AlNiCo5 magnets. The rotor includes and a carbon fiber sleeve for structural integrity. The MUT, which is currently under manufacturing, is designed as a scaled version of a VFM traction motor for hybrid and full electric vehicles. The cross section of the MUT is reported in Fig. 2, and the ratings are in Tab. I.

A. VFM Model and Complex Magnetization State

The motor model is written in the dq rotating reference frame, with the d-axis defined by the physical PM orientation. The complex Magnetization State ($\boldsymbol{MS}$) is defined as:

$$\boldsymbol{MS} = \frac{\lambda_m}{\lambda_{m,max}} \cdot e^{j\phi_{MS}} \; = \; MS \cdot e^{j\phi_{MS}} \tag{1}$$

where bold symbols indicate a vector notation, λ_m is the PM flux linkage amplitude, $\lambda_{m,max}$ is its value at 100% magnetization, MS is the magnitude of $\boldsymbol{MS}$ and ϕ_{MS} is the angle between the fundamental component of PM flux and the d-axis. In the case of uniform magnetization, λ_m is aligned with the d-axis, so ϕ_{MS}=0. The motor voltage equation and magnetic model are expressed as:

$$\boldsymbol{v}_{dq} = R_s \boldsymbol{i}_{dq} + \frac{d\boldsymbol{\lambda}_{dq}}{dt} + \omega \boldsymbol{J} \boldsymbol{\lambda}_{dq} \tag{2}$$

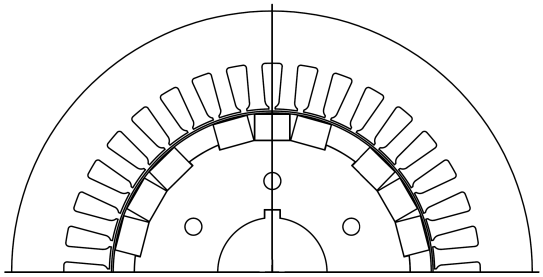

Fig. 2: Cross section of the VFM.

TABLE I: Ratings of the prototype

DC-link voltage	600 V
Maximum torque current	25 A
Maximum torque at MS 80%	35 Nm
Base speed at MS 80%	2600 rpm
Motor maximum speed	12000 rpm
Re-mag. current	70 A
Magnet	AlNiCo 5

$$\begin{cases} \lambda_d = \lambda_d\left(\boldsymbol{i}_{dq}, \boldsymbol{MS}\right) \\ \lambda_q = \lambda_q\left(\boldsymbol{i}_{dq}, \boldsymbol{MS}\right) \end{cases} \tag{3}$$

where R_s is the stator resistance, $\boldsymbol{v}_{dq}$, $\boldsymbol{i}_{dq}$ and $\boldsymbol{\lambda}_{dq}$ are the stator voltage, current and flux vectors, ω is the electrical pulsation and $\boldsymbol{J} = \begin{bmatrix} 0 & -1 \\ 1 & 0 \end{bmatrix}$ is the imaginary unit expressed in matrix form. The flux maps expressed in (3) include magnetic self- and cross-saturation at different MS. Such flux maps are shown in Fig. 3, assuming ϕ_{MS}=0. The torque Vs speed operating limits at different MS are represented as well. Noticeably, higher MS values permit higher peak torque, and field weakening is effectively obtained via MS regulation.

B. New Demag and Remag Maps in Magnitude and Phase

Low coercivity PMs can be de/remagnetized by use of sufficient current in the negative/positive d axis, but the i_q current component also affects the magnetization limits, and this is important when MS manipulations are performed under load for the sake of torque continuity. This work defines two characteristic maps in the dq current plane to model the $\boldsymbol{MS}$ variations **in magnitude and phase**, to account for asymmetrical demagnetization.

Starting with the PM fully and uniformly magnetized (MS=100%, ϕ_{MS}=0), the **Demag map** determines MS and ϕ_{MS} when the VFM is subject to a demagnetizing current in the 2nd quadrant. Similarly, the **Remag map** determines the $\boldsymbol{MS}$ when a magnetizing current vector is imposed in the 1st quadrant starting at full de-magnetization (MS = 0). These maps, reported in Fig. 4, can be determined either through FEA or experiments.

C. Magnetization maps generation

The demag and remag maps were obtained following the FEA-based methodology detailed in [26]. A series of transient magnetic simulations are performed to evaluate how the $\boldsymbol{MS}$ evolves under different current excitations in the dq plane. For each point on the Demag map, the FEA simulation starts at full PM magnetization ($\boldsymbol{MS} = 100\angle 0$) and then subjected to a current pulse in the second quadrant of the dq plane, maintained for a sufficient time to reach a steady state condition. After the pulse, the current is removed, and the new $\boldsymbol{MS}$ is measured at open circuit, thereby capturing the extent of irreversible demagnetization. Similarly, for the Remag map, the machine is initially fully demagnetized ($\boldsymbol{MS} = 0$), then exposed to a current pulse in the first quadrant. The restored $\boldsymbol{MS}$ is again captured at zero current. By systematically varying the amplitude and direction of the current pulses across the operating plane, a comprehensive characterization of both the demag and remag behavior is achieved.

D. Proposed Two-PM Magnetic Model

A novel analytical model of VFM was derived, covering the asymmetrical demagnetization phenomena. Two auxiliary axes x, y are defined at $\pm\frac{\pi}{4}$ respect to the d-axis. The PM flux linkage is divided into its projections on such axes, labeled PM_x and PM_y, and treated as the combination of **two virtual magnets with symmetric field** (see Fig. 5a). Each virtual PM has its magnetization state MS_x, MS_y. The complex $\boldsymbol{MS}$, its magnitude and phase are computed as:

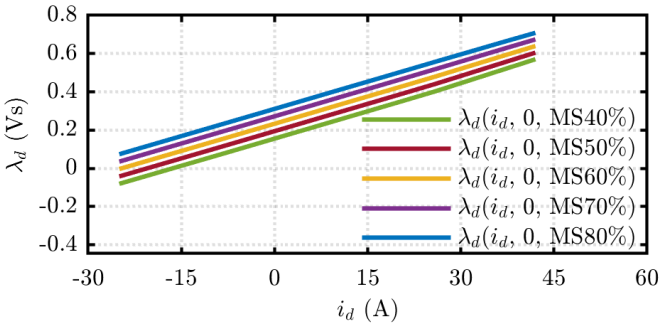

(a)

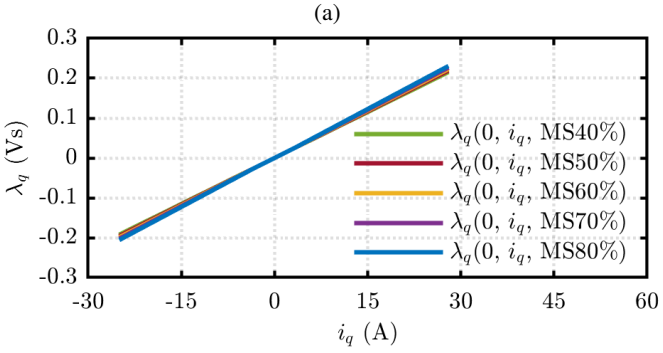

(b)

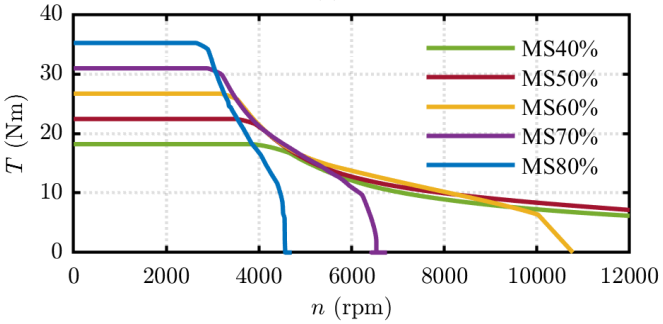

(c)

Fig. 3: FEA calculated maps for different MSs, (a) $\lambda_d\left(\boldsymbol{i}_{dq}, MS\right)$ map at ϕ_{MS}=0, (b) $\lambda_q\left(\boldsymbol{i}_{dq}, MS\right)$ map at ϕ_{MS}=0 and (c) $T - n$ profiles.

$$\begin{aligned} \boldsymbol{MS} &= \frac{1}{\sqrt{2}}\left(MS_x e^{-j\frac{\pi}{4}} + MS_y e^{j\frac{\pi}{4}}\right) \\ &= \frac{1}{2}\begin{bmatrix} MS_y + MS_x \\ MS_y - MS_x \end{bmatrix} \end{aligned} \tag{4}$$

$$MS = \frac{1}{2}\sqrt{\left(MS_x + MS_y\right)^2 + \left(MS_y - MS_x\right)^2} \tag{5a}$$

$$\phi_{MS} = \tan^{-1}\left(\frac{MS_y - MS_x}{MS_y + MS_x}\right) \tag{5b}$$

The graphical representation of the two-PM magnetic model is reported in Fig. 5a. By the inverse of (5) a Demag and a

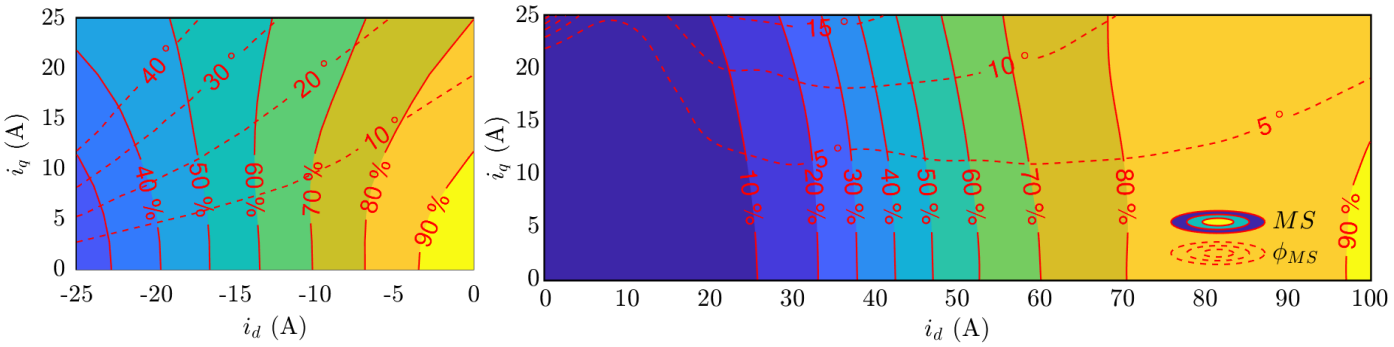

(a) (b)

Fig. 4: **MS** magnitude and phase characteristics of the MUT. (a) Demag and (b) Remag map.

Remag map are associated with each virtual PM, starting from the maps in Fig. 4. Otherwise said, the complex $\boldsymbol{MS}$ reported in Fig. 4 is converted into its cartesian components x, y. The Demag and Remag maps of PM_x and PM_y for the MUT are given in Fig. 5b and Fig. 5c.

Some remarks on the proposed two-PM model:

- the $\pm\pi/4$ orientation of the x, y axes permit capturing the ϕ_{MS} variation while preserving orthogonal coordinates.
- In principle, the model could be extended to an arbitrary larger number of PMs. Nevertheless, the test adopted for determining the demag and remag maps of the full machine present two degrees of freedom, e.g. magnitude and phase of $\boldsymbol{MS}$. A representation with more than two virtual PMs would lead to an underdetermined system.

III. Proposed Simulation Model

The proposed simulation model was developed in Matlab-Simulink, although an equivalent formulation can be implemented in other simulation environments (e.g. PLECS). It is formed by the electric motor, including its electromagnetic and mechanical models, the inverter and its discrete-time control. Among these, standard models [27], [28] are adopted for the inverter, control and mechanical model, so they will not be further treated hereafter. The key innovation regards the electromagnetic model, reported in Fig. 6.

The model input is the 3-phase inverter voltage. The Electro-Motive Force (EMF) is computed in stationary $\alpha\beta$ coordinates, and integrated to obtain the stator flux linkage $\boldsymbol{\lambda}_{\alpha\beta}$. This is rotated to obtain $\boldsymbol{\lambda}_{dq}$ and then the PM component is subtracted:

$$\boldsymbol{\lambda}_{L,dq} = \boldsymbol{\lambda}_{dq} - \boldsymbol{MS} \cdot \lambda_{m,max} \tag{6}$$

where $\boldsymbol{\lambda}_{L,dq}$ is the armature flux vector, i.e. the flux vector upon removal of the PM contribution:

$$\begin{cases} \lambda_{L,d} = \lambda_d(i_d, i_q, MS) - \lambda_d(0, 0, MS) \\ \lambda_{L,q} = \lambda_q(i_d, i_q, MS) - \lambda_q(0, 0, MS) \end{cases} \tag{7}$$

:

In the proposed model, the current vector $\boldsymbol{i}_{dq}$ is computed based on the nonlinear armature flux maps $\boldsymbol{i}_{dq} =$

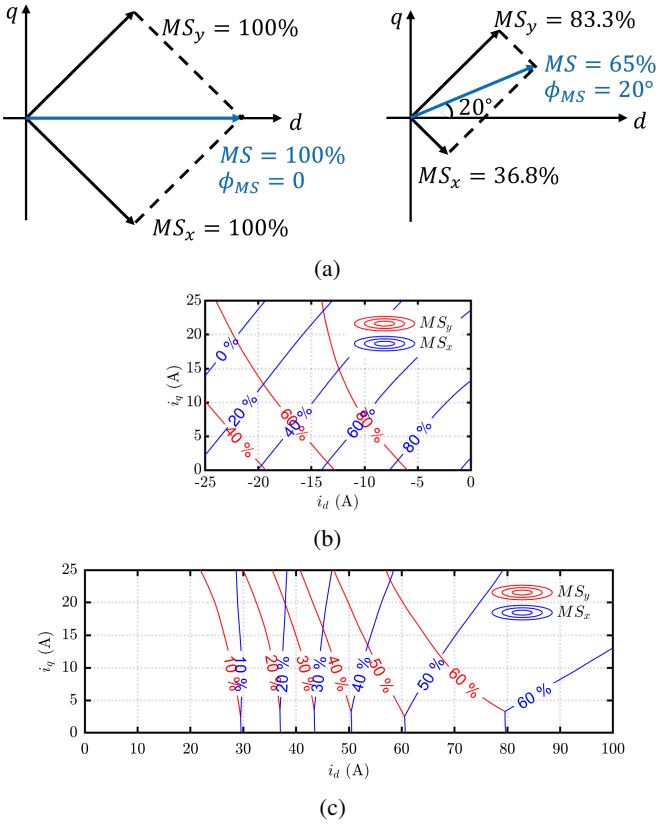

(a)

(b)

(c)

Fig. 5: (a) Vector representation of the x, y virtual magnets; (b) Demag maps for PM_x and PM_y; (c) Remag maps for PM_x and PM_y.

$\boldsymbol{i}_{dq}(\boldsymbol{\lambda}_{L,dq}, MS)$, which are obtained upon manipulation of the flux maps reported in Fig. 3 based on (7).

$$\begin{aligned} i_d &= i_d(\lambda_{L,d}, \lambda_{L,q}, MS) \\ i_q &= i_q(\lambda_{L,d}, \lambda_{L,q}, MS) \end{aligned} \tag{8}$$

f

Therefore, $\boldsymbol{\lambda}_{L,dq}$ includes magnetic self- and cross-saturation characteristics, while λ_m contribution is added on varying $\boldsymbol{MS}$.

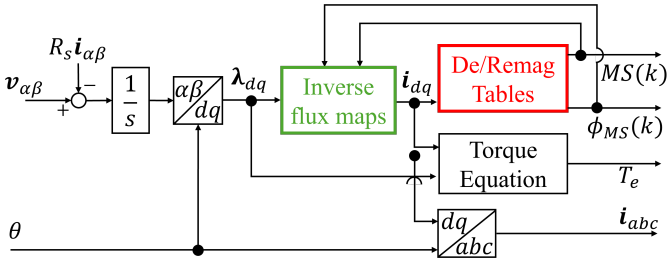

Fig. 6: Modified VFM simulation model

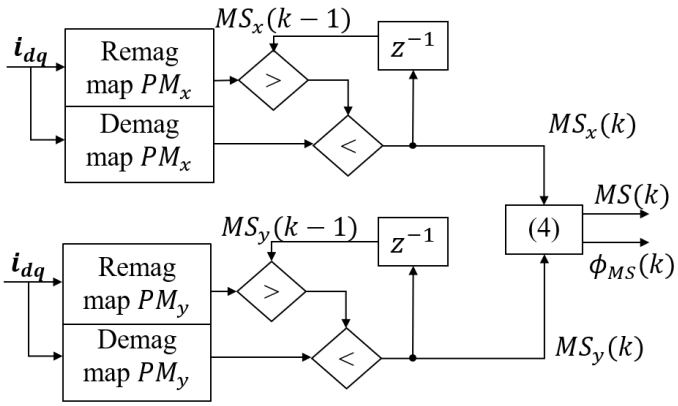

Fig. 7: Flow-chart for $\boldsymbol{MS}$ determination (red block in Fig. 6).

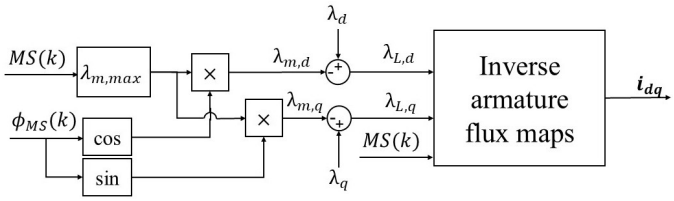

Fig. 8: Inverse flux maps (green block of Fig. 6)

The core of the proposed model are the green and red blocks of Fig. 6, capturing the saturation characteristics and the $\boldsymbol{MS}$ variations in magnitude and phase based on the Demag and Remag LUTs of PM_x and PM_y. The flow chart for $\boldsymbol{MS}$ determination is given in Fig. 7. MS_x(k) is decreased to the Demag LUT output if this is lower than the MS_x(k-1) at previous time step. Otherwise said, MS_x(k) will remain constant at MS_x(k-1) until the current vector exceeds the corresponding contour in Fig. 5b, otherwise it will decrease according to the same map. The dual approach is adopted for re-magnetization, using the Remag map of MS_x. The same principle is applied for obtaining MS_y(k). The two magnetization states are combined according to (5) to determine $\boldsymbol{MS}$(k), which is fed to the inverse armature flux map block. The magnitude of $\boldsymbol{MS}$ is used to interpolate the appropriate values from the inverse armature flux map LUTs, while $\boldsymbol{MS}$ itself is used to subtract the PM flux component from the flux obtained from the EMF integrator. The corresponding block diagram is reported in Fig. 8.

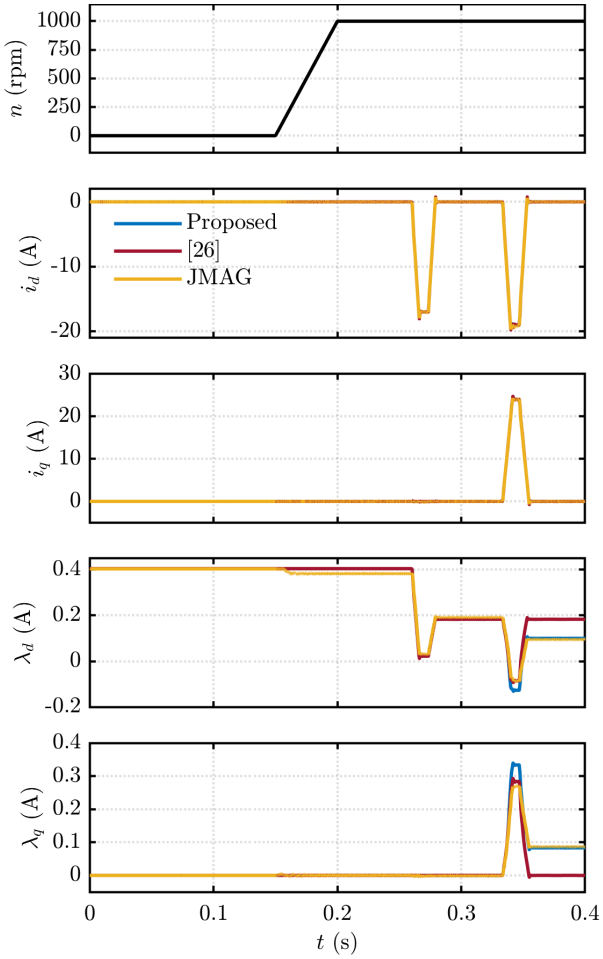

Fig. 9: Simulation results: two demagnetization pulses. Blue: proposed model; Red: symmetric model in [26]; Yellow: JMAG FEA simulation.

IV. Simulation Results

The proposed simulation model is validated by comparison against transient FEA simulations carried in JMAG Designer [29] environment and against the Simulink symmetric MS model in [26]. In the two Simulink models, the VFM is closed loop current controlled, whereas the current waveform is directly imposed in JMAG.

An example of results is reported in Fig. 9, with the machine externally driven at 1000 rpm and starting with $\boldsymbol{MS} = 100\angle 0$. A first, symmetric demagnetization pulse is applied at i_d =-17 A, i_q=0 A and released, followed by a second asymmetric demagnetization using i_d =-19 A, i_q=24 A, also released. The dq current and flux linkage waveforms are represented for the three models. The model in [26] captures the symmetric pulse but fails to capture that the PMs are asymmetrically demagnetized at the end of the second pulse, as witnessed by the non-zero λ_q component of the flux linkage (Fig. 9). In contrast, the proposed model tracks the FEA results and the deviated PM flux with negligible steady-state error and minimal transient discrepancy.

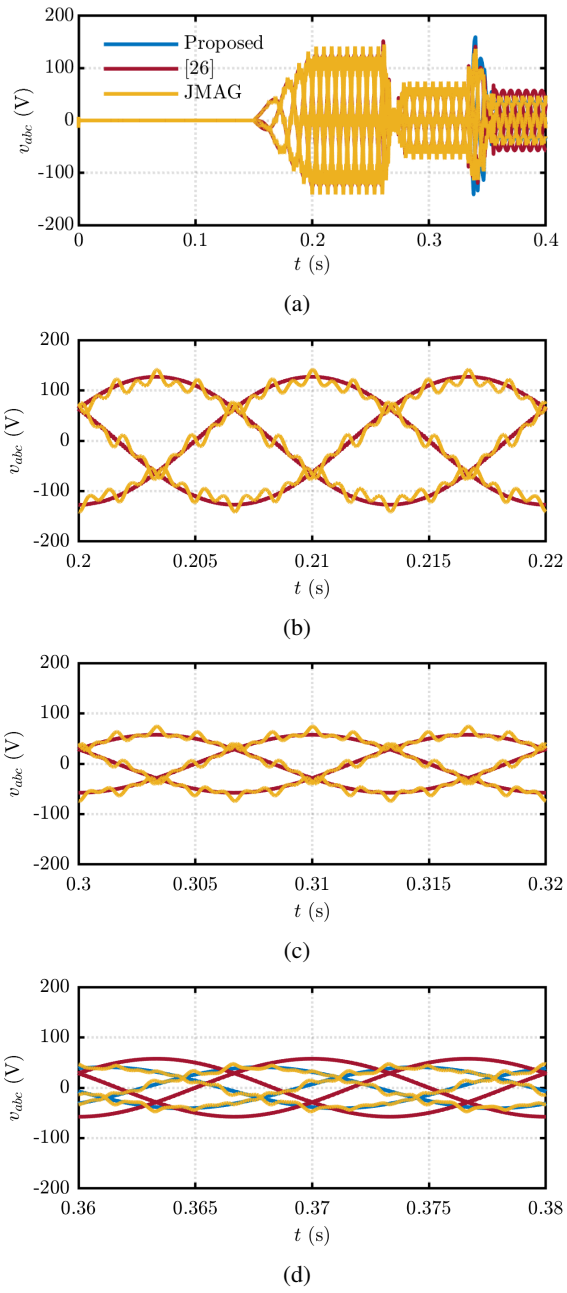

Fig. 10: Open circuit voltage waveforms at different stages of the demagnetization process. Simulation results: two demagnetization pulses. Blue: proposed model; Red: symmetric model in [26]; Yellow: JMAG FEA simulation. (a) Complete time waveform; (b) detail before the first demagnetization pulse; (c) detail after the first symmetrical demagnetization; (d) detail after the asymmetrical demagnetization pulse.

Beyond the flux analysis, Fig. 10 reports the details of the machine's back-EMF waveform before the demagnetization (Fig. 10b), after the symmetrical demagnetization pulse (Fig. 10c) and after the second, asymmetrical demagnetizing pulse (Fig. 10d). As can be noted, the model in [26] correctly captures the EMF after the first current pulse, but it fails

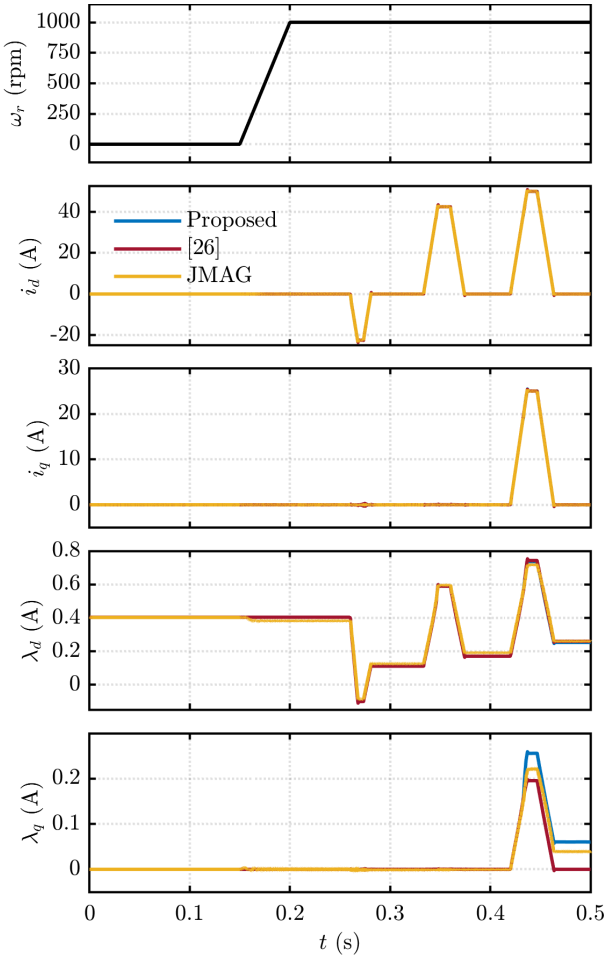

Fig. 11: Simulation results: demagnetization pulse followed by two remagnetization pulses. Blue: proposed model; Red: symmetric model in [26]; Yellow: JMAG FEA simulation.

tracking the second pulse, showing an EMF phase shift of 40° and a magnitude overestimation of 40%. Conversely, the proposed model is coherent with the JMAG reference during the full simulation. The only noticeable difference lies in the space harmonic content, which is modeled in the JMAG FEA and omitted in Simulink. This approximation is generally accepted for motor control development.

A second test, depicted in Fig. 11, was carried simulating a remagnetization transient. The test started again from a fully magnetized machine ($\boldsymbol{MS} = 100\angle 0$). A first symmetrical demagnetization pulse (i_d =-22.5 A, i_q=0 A) is applied and released, followed a symmetric remagnetization pulse (i_d =42.5 A, i_q=0 A) and an asymmetric pulse (i_d =50 A, i_q=25 A). The first pulse symmetrically demagnetizes the machine to $\boldsymbol{MS} = 30\angle 0$. The first remagnetization pulse leads to $\boldsymbol{MS} = 40\angle 0$, and the last pulse to $\boldsymbol{MS} = 65\angle 13.5°$. Again, the model in [26] correctly tracks the symmetrical pulses, but fails representing the asymmetrical magnetization, which is instead included in the proposed model. This is further confirmed by the EMF waveforms reported in Fig. 12,

depicting the details of open circuit voltage at each magnetization stage.

Finally, the computational burden of the proposed model is compared against the FEA-based simulation in terms of execution time and storage demand, demonstrating a significant improvement. The results are shown in Tab. II. All simulations were executed on the same workstation with a system configuration of 32GB RAM, an Intel Core i9-12900 processor @2.50GHz and 1TB NVMe SSD. The proposed Simulink model was executed 10 times, averaging the simulation time over the different iterations, both for the Demag and the Remag tests. Due to the heavy computations involved at each time step in the FEA model, which need to generate large-sized files, the step time in JMAG was set to be an order of magnitude larger than in Simulink, owing to space and time limitations. While Simulink used a variable step time limited to $2\mu s$, the JMAG simulations were run with step times of $20\mu s$ for the Demag test and $50\mu s$ for the Remag test. Despite the considerably larger time step, the proposed model reduces the computational time by $\approx$500 times, and the storage demand by three orders of magnitude. Overall, the results demonstrates that the proposed model can effectively reduce the simulation time with minimal loss in accuracy when compared to FEA-based cosimulaiton approaches.

It is also worth highlighting that the phase current was directly imposed in the FEA simulation. If the motor control and inverter models were included, as is done in Simulink, the required simulation time would have been significantly higher.

V. Conclusions

In VFMs, magnetization state transients under load can lead to asymmetrical demagnetization of the PMs, a phenomenon typically analyzed using computationally intensive FEA or co-simulation methods. This work introduces an enhanced analytical magnetic model capable of accurately capturing such asymmetrical demagnetization effects. The model is integrated into a fast dynamic simulation framework suitable for control development and calibration tasks. Compared to traditional FEA-based co-simulations, the proposed approach offers a substantial improvement in computational efficiency, reducing simulation time by approximately 500× and memory requirements by three orders of magnitude, without compromising accuracy. The methodology is validated using an SPM VFM prototype, designed as a down-scaled proof-of-concept for traction applications, confirming its effectiveness and practical relevance for fast, accurate simulation and control design.

The proposed model was developed in Matlab-Simulink. Anyway, being a fully LUT-based model, the same approach can be adopted in other simulation environments, such as PLECS.

Acknowledgment

This publication is part of the project PNRR-NGEU which has received funding from the MUR-DM 352/2022 and Volvo Car Cooperation.

The research has been conducted with the support of Power Electronics Innovation Center (PEIC) of Politecnico di Torino.

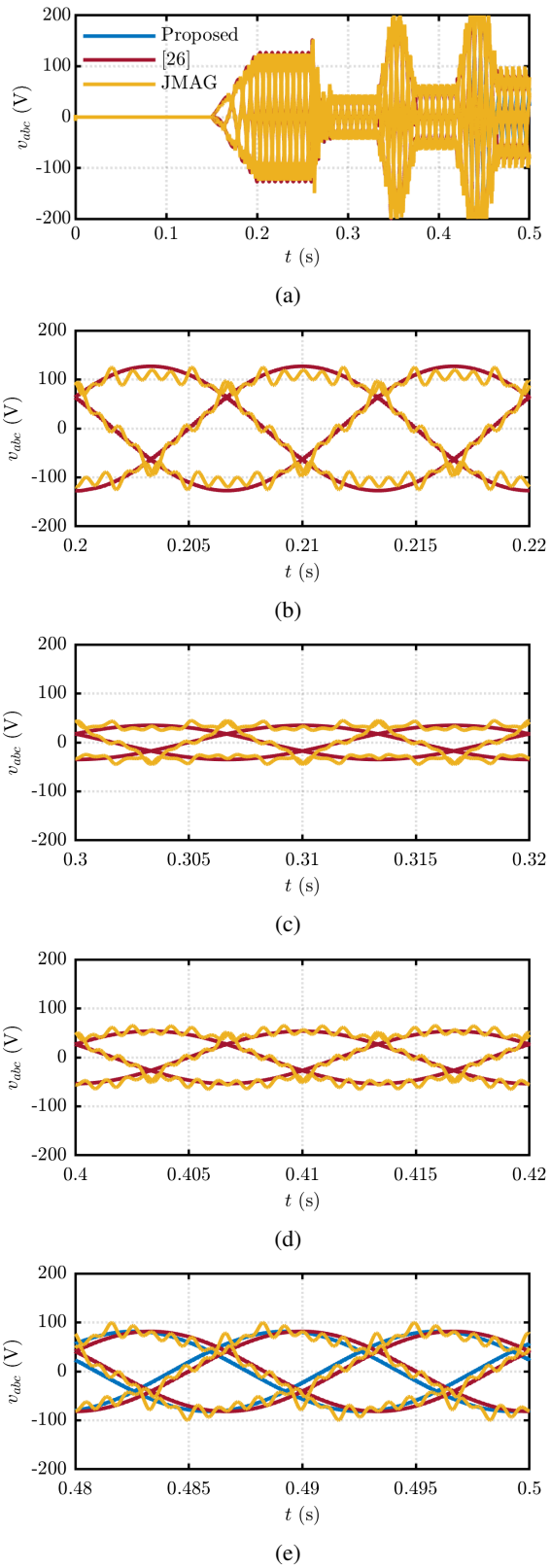

Fig. 12: Open circuit voltage under two remagnetization pulses. Blue: proposed model; Red: symmetric model in [26]; Yellow: JMAG FEA simulation. (a) Complete time waveform; (b) detail before demag.; (c) after symmetrical demag.; (d) after symmetrical remag.; (e) after asymmetrical remag.

TABLE II: Model performance assessment

Modeling Approach	Computational Time		Storage Demand	
	Demag Test	Remag Test	Demag Test	Remag Test
Proposed Simulink Model	≈11s	≈14s	≈27MB	≈27MB
FEA-based (JMAG 23.1)	≈75min	≈124min	≈46GB	≈23GB

REFERENCES

[1] P. Ramesh and N. C. Lenin, "High power density electrical machines for electric vehicles—comprehensive review based on material technology," *IEEE Transactions on Magnetics*, vol. 55, no. 11, pp. 1–21, 2019.

[2] P. Pescetto, G. Dilevrano, F. Stella, G. Pellegrino, and A. Boglietti, "Enhanced short-time thermal transient model and testing procedure for high power density motors, such as in supercar traction," *IEEE Open Journal of Industry Applications*, vol. 6, pp. 391–402, 2025.

[3] A. Credo, G. Fabri, M. Villani, and M. Popescu, "Adopting the topology optimization in the design of high-speed synchronous reluctance motors for electric vehicles," *IEEE Transactions on Industry Applications*, vol. 56, no. 5, pp. 5429–5438, 2020.

[4] Z. Q. Zhu and D. Howe, "Electrical machines and drives for electric, hybrid, and fuel cell vehicles," *Proceedings of the IEEE*, vol. 95, no. 4, pp. 746–765, 2007.

[5] A. Quesada, "The permanent magnets challenge," *Instituto de Ceramica y Vidrio, icv*, vol. 50, 2014.

[6] A. Chiba, K. Kiyota, N. Hoshi, M. Takemoto, and S. Ogasawara, "Development of a rare-earth-free sr motor with high torque density for hybrid vehicles," *IEEE Transactions on Energy Conversion*, vol. 30, no. 1, pp. 175–182, 2015.

[7] A. Credo and P. Pescetto, "A systematic method for the calibration of fea model of synchronous reluctance machines considering manufacturing effects," *IEEE Open Journal of Industry Applications*, pp. 1–12, 2025.

[8] H. Chen, J. Tang, Y. Liu, B. Jiang, and L. Boscaglia, "Electromagnetic performance investigation of a brushless electrically excited synchronous machine for long-distance heavy-duty electric vehicles," *IEEE Transactions on Transportation Electrification*, vol. 11, no. 1, pp. 225–235, 2025.

[9] R. Leuzzi, P. Cagnetta, F. Cupertino, S. Ferrari, and G. Pellegrino, "Performance assessment of ferrite- and neodymiumassisted synchronous reluctance machines," in *2017 IEEE Energy Conversion Congress and Exposition (ECCE)*, 2017, pp. 3958–3965.

[10] V. Ostovic, "Memory motors," *IEEE Industry Applications Magazine*, vol. 9, no. 1, 2003.

[11] R. Tu, H. Yang, H. Lin, H. Zhan, D. Wu, and M. Yu, "Design and optimization of a novel delta-type consequent-pole hybrid magnet memory machine," *IEEE Transactions on Energy Conversion*, vol. 39, no. 2, pp. 1265–1277, 2024.

[12] N. Limsuwan, T. Kato, K. Akatsu, and R. D. Lorenz, "Design and evaluation of a variable-flux flux-intensifying interior permanent magnet machine," in *2012 IEEE Energy Conversion Congress and Exposition (ECCE)*, 2012, pp. 3670–3677.

[13] H. Yang, W. Liu, H. Zheng, H. Lin, Z. Q. Zhu, F. Peng, Y. Li, S. Lyu, and X. Huang, "A novel delta-type hybrid-magnetic-circuit variable flux memory machine for electrified vehicle applications," *IEEE Transactions on Transportation Electrification*, vol. 8, no. 3, pp. 3512–3523, 2022.

[14] K. Yoneda, W. Suzuki, and K. Sakai, "Designing a leaf-benchmark variable magnetization-ipm motor with two v-shaped pms at a 100 kw power level," in *2022 IEEE Energy Conversion Congress and Exposition (ECCE)*, 2022, pp. 1–7.

[15] A. Athavale, K. Sasaki, B. S. Gagas, T. Kato, and R. D. Lorenz, "Variable flux permanent magnet synchronous machine (vf-pmsm) design methodologies to meet electric vehicle traction requirements with reduced losses," *IEEE Transactions on Industry Applications*, vol. 53, no. 5, pp. 4318–4326, 2017.

[16] Y. Hu, B. Chen, Y. Xiao, X. Li, Z. Zhang, J. Shi, and L. Li, "Research and design on reducing the difficulty of magnetization of a hybrid permanent magnet memory motor," *IEEE Transactions on Energy Conversion*, vol. 35, no. 3, pp. 1421–1431, 2020.

[17] S. Maekawa, K. Yuki, M. Matsushita, I. Nitta, Y. Hasegawa, T. Shiga, T. Hosoito, K. Nagai, and H. Kubota, "Study of the magnetization method suitable for fractional-slot concentrated-winding variable magnetomotive-force memory motor," *IEEE Transactions on Power Electronics*, vol. 29, no. 9, pp. 4877–4887, 2014.

[18] Y. Hu, B. Chen, Y. Xiao, X. Li, J. Chen, and H. Fang, "Comprehensive control of a hybrid-magnet variable-flux memory machine for washing machine applications," in *2021 IEEE 4th International Electrical and Energy Conference (CIEEC)*, 2021, pp. 1–6.

[19] J. H. Lee, J.-Y. Song, H.-K. Yeo, and S.-Y. Jung, "Numerical evaluation of a concentrated-winding variable flux memory motor with a hybrid magnet arrangement," *IEEE Access*, vol. 11, pp. 71 756–71 765, 2023.

[20] C. Yu, S. Niu, S. L. Ho, W. Fu, and L. Li, "Hysteresis modeling in transient analysis of electric motors with alnico magnets," *IEEE Transactions on Magnetics*, vol. 51, no. 3, pp. 1–4, 2015.

[21] C. Schulte and J. Böcker, "Co-simulation of an electric traction drive," in *2013 International Electric Machines Drives Conference*, 2013, pp. 974–978.

[22] H. Yang, H. Zheng, S. Lyu, H. Lin, Z.-Q. Zhu, and W. Fu, "Analysis of flux regulation principle in a novel hybrid-magnet-circuit variable flux memory machine," in *2019 22nd International Conference on Electrical Machines and Systems (ICEMS)*, 2019, pp. 1–6.

[23] B. Basnet and P. Pillay, "Co-simulation based electric vehicle drive for a variable flux machine," in *2020 IEEE Transportation Electrification Conference Expo (ITEC)*, 2020, pp. 1133–1138.

[24] K. S. Amitkumar, R. Thike, and P. Pillay, "Power-hardware-in-the-loop based emulation of a variable flux machine," in *2018 IEEE Energy Conversion Congress and Exposition (ECCE)*, 2018, pp. 6454–6460.

[25] R. Thike and P. Pillay, "Parameter measurements and modeling of a novel hybrid variable flux machine with series rare-earth and alnico magnets," in *2020 IEEE Energy Conversion Congress and Exposition (ECCE)*, 2020, pp. 1433–1438.

[26] M. S. Mirazimi, C. Chen, P. Pescetto, S. Ferrari, G. Pellegrino, M. Diana, and T. Thiringer, "Accurate modeling of variable- flux pmsms without electromagnetic co-simulation," in *2024 International Symposium on Power Electronics, Electrical Drives, Automation and Motion (SPEEDAM)*, 2024, pp. 625–630.

[27] C. Chen, P. Pescetto, S. Ferrari, G. F. Olson, M. Diana, T. Thiringer, and G. Pellegrino, "Fast determination of feasible torque-speed range for variable flux machines including remagnetization voltage limit," in *2025 IEEE Energy Conversion Congress and Exposition (ECCE)*, 2025.

[28] A. Varatharajan, D. Brunelli, S. Ferrari, P. Pescetto, and G. Pellegrino, "syredrive: Automated sensorless control code generation for synchronous reluctance motor drives," in *2021 IEEE Workshop on Electrical Machines Design, Control and Diagnosis (WEMDCD)*, 2021, pp. 192–197.

[29] "JMAG-Designer." [Online]. Available: https://www.jmag-international.com/products/jmag-designer/